Acta Oceanol. Sin., 2018, Vol. 37, No. 7, P. 8–19
DOI: 10.1007/s13131-018-1240-2
http://www.hyxb.org.cn
E-mail: hyxbe@263.net

Relationships between intensity of the Kuroshio current in the East China Sea and the East Asian winter monsoon

YIN Ming[1, 3], LI Xin[2, 3], XIAO Ziniu[2], LI Chongyin[2, 3*]

[1] Army 61936 of PLA, Haikou 571100, China

[2] Institute of Atmospheric Physics, Chinese Academy of Sciences, Beijing 100029, China

[3] Institute of Meteorology & Oceanography, National University of Defense Technology, Nanjing 211101, China

Received 16 August 2017; accepted 26 September 2017

Abstract

Based on satellite altimeter and reanalysis data, this paper studies the relationships between the intensity of the Kuroshio current in the East China Sea (ECS) and the East Asian winter monsoon (EAWM). The mechanisms of their possible interaction are also discussed. Results indicate that adjacent transects show consistent variations, and on an interannual timescale, when the EAWM is anomalously strong (weak), the downstream Kuroshio in the ECS is suppressed (enhanced) in the following year from February to April. This phenomenon can be attributed to both the dynamic effect (i.e., Ekman transport) and the thermal effect of the EAWM. When the EAWM strengthens (weakens), the midstream and downstream Kuroshio in the ECS are also suppressed (intensified) during the following year from October to December. The mechanisms vary for these effects. The EAWM exerts its influence on the Kuroshio's intensity in the following year through the tropospheric biennial oscillation (TBO), and oceanic forcing is dominant during this time. The air-sea interaction is modulated by the relative strength of the EAWM and the Kuroshio in the ECS. The non-equivalence of spatial scales between the monsoon and the Kuroshio determines that their interactions are aided by processes with a smaller spatial scale, i.e., local wind stress and heating at the sea surface.

Key words: East Asian winter monsoon, Kuroshio intensity, East China Sea, interaction, correlation analysis, composite analysis

Citation: Yin Ming, Li Xin, Xiao Ziniu, Li Chongyin. 2018. Relationships between intensity of the Kuroshio current in the East China Sea and the East Asian winter monsoon. Acta Oceanologica Sinica, 37(7): 8–19, doi: 10.1007/s13131-018-1240-2

1 Introduction

The most important ocean current in the western North Pacific, the Kuroshio, originates from the northern branch of the North Equatorial Current (NEC). After bifurcating from the NEC off the Philippines, it passes the Luzon Strait and continues flowing northwards along the eastern coast of Taiwan (Hsin et al., 2013). The Kuroshio enters the East China Sea (ECS) through the East Taiwan Channel, and after flowing northward along the Chinese continental shelf, the Kuroshio separates from the Japan coast and turns eastward about 35°N. Through over more than half a century of investigations, researchers worldwide have developed a preliminary understanding of the characteristics (i.e., transport, intensity, axis, depth and frequency of variability) of the Kuroshio in different regions. The many factors influencing the Kuroshio include submarine topography, mesoscale eddy, local and non-local wind stress, El Niño-Southern Oscillation (ENSO), and Pacific Decadal Oscillation (PDO) (Yang et al., 1999; Qiu, 1999; Johns et al., 2001; Chang and Oey, 2011, 2012; Qiu and Chen, 2010, 2013).

The Kuroshio is renowned for its huge transport, strong intensity, narrow width and deep depth; and its physical characteristics of high temperature, high salinity, and dark blue transparent water. Through the interchange of momentum, energy, and material, the Kuroshio exerts a remarkable influence on circulation in the China's seas, and is the main driver of offshore circulation.

In general, the formation of the monsoon system is mainly attributed to wind reversal caused by seasonal variation in the thermal contrast between land and sea (Chen et al., 2006). On the one hand, located in the monsoon region and the main area of heat loss from the world's oceans (Huang, 2012), the Kuroshio transfers huge amounts of energy to the atmosphere. This significantly affects atmospheric circulation (including the monsoon system) and climate change (Xu et al., 2008, 2011; Hu et al., 2015). On the other hand, in the mid-latitudes, especially in the boreal winter, atmospheric forcing on the ocean cannot be ignored (Wallace and Jiang, 1987; Li et al., 2011b), such that the monsoons also modulate the volume and heat transport of the Kuroshio itself. Thus, complex interactions exist between the Kuroshio and the East Asian monsoon. This work focuses on the processes operating during the boreal winter, while interactions during the summer will be reported in subsequent articles.

Many previous studies have investigated the relationships between thermal conditions in the Kuroshio, the East Asian general circulation and the climate of China (Qin and Sun, 2006; Zhang et al., 2008; Sasaki et al., 2012; Soeyanto et al., 2014). Representative of many investigations, Li and Long (1992) pointed out that positive SST anomalies cause precipitation to increase

Foundation item: The National Basic Research Program (973 program) of China under contract No. 2013CB956200; the National Natural Science Foundation of China under contract Nos 41490642 and 41605051.
*Corresponding author, E-mail: lcy@lasg.iap.ac.cn

during the flood season over northern and northeastern China. Through statistical analysis, Li and Ding (2002) found that when the Kuroshio region has a positive SST anomaly, summer rainfall over the Changjiang (Yangtze) River valley and the temperature in most of Eurasia also have positive anomalies. Liang et al. (2006) reported that air–sea heat fluxes are significantly anomalous in the East Asian coastal area under the effect of the East Asian winter monsoon (EAWM). In comparison, relatively little work has been concerned with dynamic forcing of the monsoon, especially local wind stress, and most studies have focused on seasonal timescales (Chuang and Liang, 1994; Oey et al., 2010; Chang and Oey, 2012). For instance, Wang et al. (2010) suggested that different prevailing winds in winter and summer have different influences on the gap-leaping western boundary current. There are few existing studies connecting the EAWM with the Kuroshio in the ECS over interannual timescales from both thermal and dynamic perspectives.

Furthermore, because of the lack of *in situ* hydrological data, only variations in the Kuroshio's transport at specific transects can be analyzed. (Along its pathway in the ECS, the transect is usually named PN; its position is mapped in Fig. 1). However, strong eddies and internal tides in the Kuroshio may cause substantial contrast in transport for two adjacent transects. In this study, using high-resolution altimetric data, the geostrophic intensity is calculated at seven transects covering the Kuroshio in the ECS, allowing variations to be studied in detail, and revealing interannual relationships with the EAWM.

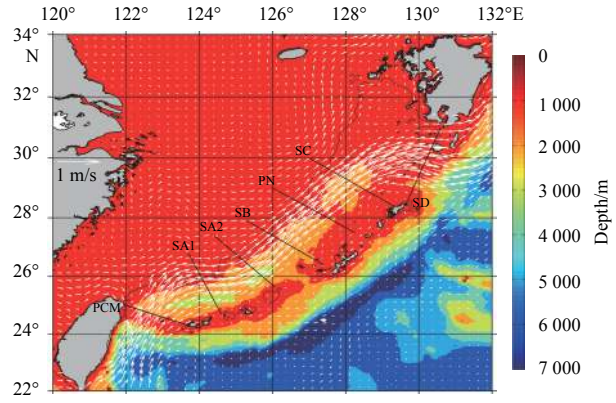

Fig. 1. The terrain of the East China Sea and adjacent waters (shading), altimeter-derived climatological mean geostrophic current field (arrows), and the selected research transects (black lines).

This paper is arranged into four sections. In Section 2, the data and methods of analysis adopted in this study are described. Results are presented in Section 3. A discussion and conclusions make up the final section.

2 Data and methods

This paper uses the following data: state-of-the-art versions of Maps of Absolute Dynamic Topography (MADT) are provided by AVISO (Archiving Validation and Interpretation of Satellite Oceanographic data; http://www.aviso.oceanobs.com/). The data are gridded on a 1-day time interval and a Cartesian grid of (1/4)°×(1/4)°, covering the period 1 January 1993 to 31 December 2012. The NCEP_Reanalysis 2 data of the daily wind field at 850 hPa and the monthly wind field at 10 m, provided by the NOAA/OAR/ESRL PSD, Boulder, Colorado, USA, from their web site at http://www.esrl.noaa.gov/psd/ are also utilized. Monthly ocean surface heat flux and temperature products are provided by WHOI (Woods Hole Oceanographic Institution; http://oaflux.whoi.edu/heatflux.html) (Yu and Weller, 2007). For uniformity, the timespan of all variables is consistent with the MADT data.

The intensity and transport of the Kuroshio can be expressed by both the tide gauge-derived sea surface height anomaly and the altimeter-derived geostrophic velocity (Hsin et al., 2013). The former serves as a proxy as proven by correlation analysis, while the latter is a more reliable quantitative analysis. In this paper, the second method was chosen, as proposed by Hsin et al. (2013) when they studied seasonal to interannual intensity variations in the surface Kuroshio east of Taiwan. Based on the geostrophic balance, surface geostrophic velocities in the Kuroshio in the ECS are calculated from the MADT as follows:

$$u_g(x, y, t) = -\frac{g}{f(y)}\frac{\partial h(x, y, t)}{\partial y},$$
$$v_g(x, y, t) = -\frac{g}{f(y)}\frac{\partial h(x, y, t)}{\partial x},$$

where x, y and t are longitude, latitude and time, respectively; u_g and v_g are the zonal and meridional components of the geostrophic current, respectively; h is the absolute dynamic topography; g is gravitational acceleration; $f(y) = 2\Omega \sin y$ is the Coriolis parameter, and Ω is the angular velocity of the Earth's rotation. The surface Kuroshio intensity ($\mathrm{INT_g}$) at a specific transect can be calculated by

$$\mathrm{INT_g} = \int_{L_s}^{L_e} \vec{V}_g \cdot \mathrm{d}\vec{l},$$

where $\vec{V}_g$ is the geostrophic current vector; $\mathrm{d}\vec{l}$ is the infinitesimal element of the normal vector of the Kuroshio transect; L_s and L_e are the start and end points of the Kuroshio section, respectively.

To fully reflect the Kuroshio's intensity variation in the ECS, the $\mathrm{INT_g}$ at transects from PCM to SD was calculated, all of which are designed to span the Kuroshio along its path (Fig. 1). Transects PCM, SA1 and SA2 are located in the upstream ECS Kuroshio, transects SB and PN in the midstream, and transects SC and SD are downstream. These transects are chosen referring to Soeyanto et al. (2014). Transects PCM and PN are named following usual conventions (Hsin et al., 2013), and other transects are named for brevity.

Wavelet and power spectral analyses at each transect (figure omitted) indicate that the $\mathrm{INT_g}$ along the Kuroshio is dominated by intraseasonal variations at timescales below 100 d, caused by both the bottom topography and impinging westward-propagating mesoscale eddies originating in the interior Pacific (Yang et al., 1999; Qiu, 1999; Johns et al., 2001). Another significant period is annual change, due to monsoons and heat fluxes over the shelf region (Chao, 1990; Oey et al., 2010). Additionally, at SB and PN, there is a distinct oscillation of 2–3 a. However, intraseasonal and annual changes are not the main concern here. In this paper, the focus will be on interannual relationships between the Kuroshio $\mathrm{INT_g}$ in the ECS and the East Asian winter monsoon. Dynamic height noise associated with high-frequency activities can be largely filtered out by averaging (Wijffels et al., 1995), so the monthly mean of the daily $\mathrm{INT_g}$ is calculated and adopted as the parameter in this research.

The INT_g at transects in the same region presents a consistent variation. This is confirmed by the relatively high correlations between any two of them (Table 1), which, although not as high as expected, still pass the 95% significance test. In contrast, the INT_g shows different features in different regions, and the INT_g correlation between midstream and upstream transects is not as significant as between midstream and downstream transects.

An appropriate indicator for the East Asian monsoon needs to be applied in order to study its relationship with the Kuroshio's intensity. In this work, the unified East Asian monsoon index (EAMI) described by Li et al. (2011a) was used. The process involves averaging southwest–northeast wind velocity in the domain of grid points within the study area 10°–22.5°N and 110°–122.5°E. The normalized data are then calculated as below:

$$EAMI = \frac{V}{\sqrt{\frac{\sum V^2}{n}}},$$

where the regional mean V stands for $(u+v)/\sqrt{2}$, u and v are the zonal and meridional winds, respectively, and n is the sample number. Accordingly, the daily EAMI from 1 January 1993 to 31 December 2012 were obtained using the NCEP wind data at 850 hPa.

Figure 2a illustrates seasonal variation in the EAMI climatology. The basic circulation of the East Asian monsoon is consistent with that given by Li et al. (2011a). In general, the East Asian summer monsoon onsets in late May, and the East Asian winter monsoon is established in late October. The transition between summer and winter monsoons agrees with observations. Using this simple index, the relationships between the winter monsoon and the Kuroshio INT_g at the selected transects in the ECS were analyzed.

The December-to-February 3-month mean EAMI were selected to represent winter conditions in a composite analysis. The time series of the normalized winter EAMI is given in Fig. 2b. Here, 1993 indicates the 1993/1994 winter, and similar labels are applied to subsequent years. It is clear that the winter monsoon possesses a pronounced inter-annual variation. Winter EAMI values greater than half the standard deviation from the average are therefore selected as weak winter monsoon cases. Four weak winter monsoon cases (1997, 2002, 2004 and 2009) were identified. Similarly, winter EAMI values less than half the standard deviation from the average are chosen as strong winter monsoon cases. The six selected strong winter monsoon cases are 1995, 1998, 1999, 2006, 2007 and 2008.

3 Results and discussion

3.1 *Lead/lag correlations between winter EAMI and INT_g*

The lead/lag correlations between the winter EAMI and the Kuroshio INT_g for each transect are calculated. The procedure for calculating the correlation coefficients is as follows: (1) extract the monthly winter EAMI values from December to February and arrange them chronologically; (2) extract the monthly intensity which leads/lags particular months of the three winter months and arrange them in the same way; and (3) calculate the coefficient between the two sequences.

For equivalent periods, the performance of each transect is

Table 1. Correlation coefficients of INT_g between pairs of transects

	PCM	SA1	SA2	SB	PN	SC	SD
PCM		0.62	0.39	0.16	0.17	0.26	0.29
SA1			0.71	0.36	0.22	0.18	0.22
SA2				0.53	0.35	0.28	0.28
SB					0.77	0.54	0.48
PN						0.74	0.63
SC							0.82
SD							

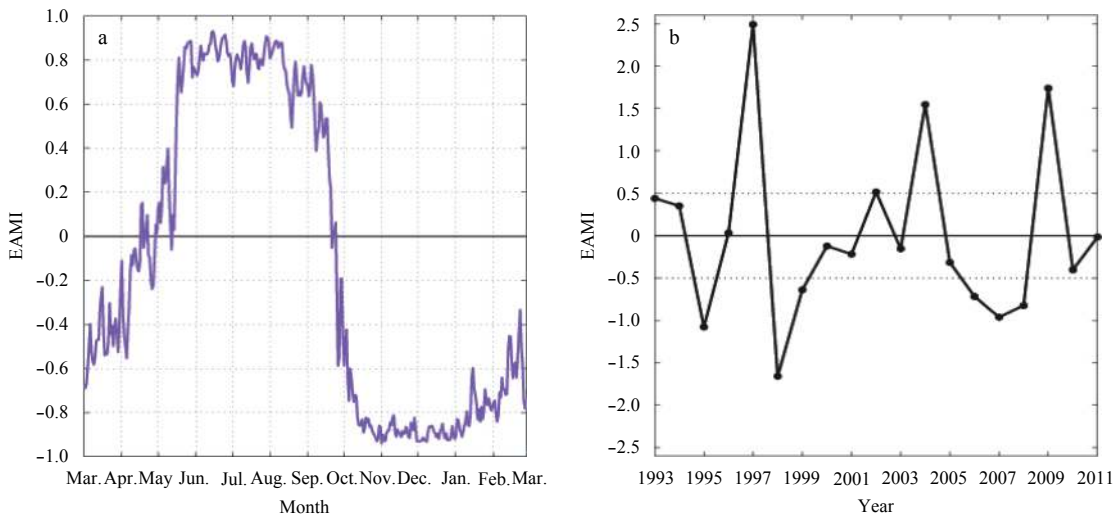

Fig. 2. Seasonal variation of the climatological EAMI (1993–2012; based on daily data) (a), and time series of the normalized winter EAMI (1993–2011) (b).

mostly consistent (Tables 2 and 3). For instance, leading the winter by 11 months, the INT_g from January to March at all transects is positively correlated with the winter EAMI; the INT_g leading the winter by approximately 4–5 months is negatively correlated with the winter EAMI; lagging 2 and 10 months behind the winter, the INT_g during February to April and October to December in the following year is positively correlated with the winter EAMI. At other times, although certain transects show some inconsistency, such as SA2 leading the winter by 9 months, and PCM and SA2 lagging the winter by 5 months, consistent signs are otherwise maintained for transects close to one another (e.g., SB to SD leading 10 and 6 months, PN to SD leading 3 months, and PCM to SA2 lagging 7 months). The analysis suggests that for most periods the variation in features is consistent between transects, and that transects in the same region have similar variations. However, there are periods when INT_g variations in the upstream, midstream and downstream Kuroshio are not synchronized. A detailed analysis of this will be given in the following section.

3.2 *Interaction between the Kuroshio intensity in the ECS and the EAWM*

This section discusses the relationship between the Kuroshio INT_g in the ECS and the EAWM. For clarity, the main focus is on when these indices are significantly correlated—i.e., early spring (February to April) and winter (October to December).

3.2.1 *Impacts of the EAWM on the Kuroshio intensity in the ECS in the following early spring*

The lag-correlation results show that the winter EAMI is positively correlated with the 2-month-lag INT_g at Transects SC and SD, significant at the 90% level. This suggests that the INT_g in the downstream ECS Kuroshio is related to the EAWM to some extent. To see this clearly, the spatial distribution of correlation coefficients between the winter southwest–northeast wind speed field and the INT_g in the following February–April at seven transects is given in Fig. 3. The figure shows high positive correlations at Transects PCM, SC and SD in the monsoon region. This means that when the southwesterly winds strengthen (winter monsoon weakens), the INT_g at PCM, SC and SD intensifies, and vice versa. This result is consistent with that of the lag-correlations above. Given that the PCM transect is far from downstream, and its 2-month-lag-correlation coefficient is not high enough to be significant (Table 3), it will not be discussed here. The composites of the 3-month running mean INT_g after the strong and weak winter monsoons at SC and SD (Fig. 4) show that the INT_g at these two transects (or downstream) is indeed weaker from February to April after strong winter monsoons than after weak monsoons. To determine how the winter monsoon exerts its influence on the Kuroshio over the following months, the mechanisms from thermal and dynamic aspects were analyzed.

3.2.1.1 *Thermal process*

Composites of turbulent heat fluxes (sensible and latent) for different winter monsoon conditions are given in Fig. 5. There is a high-value belt where the Kuroshio releases much more heat to the atmosphere than in the neighboring vicinity (Fig. 5a). Under strong winter monsoon conditions, there is a positive anomaly covering the Kuroshio in the ECS, with extremes centered in the downstream region. Thus, the downstream Kuroshio releases more turbulent heat flux to the atmosphere in the following February–April period (Fig. 5b). In strong contrast, the anomaly is negative in weak monsoon cases and the Kuroshio in the ECS releases less heat to atmosphere (Fig. 5d).

To understand the flux anomalies, the combined behavior of wind speed, the air–sea temperature difference (ΔT), and the ocean surface saturation humidity–air humidity difference (Δq) must be included. Figure 6a shows the wind anomaly under strong winter monsoon conditions. An anomalous northeasterly exists over the Kuroshio and the wind speed is greater. Under weak winter monsoon conditions (Fig. 6b), the anomaly changes to southwesterly and the wind speed is lower.

Because ΔT and Δq are correlated (cooler air is usually drier, especially outside the tropics) (Cayan, 1992), ΔT is used as the

Table 2. Leading correlation coefficients of the INT_g with the winter EAMI

	–11 (Jan.)	–10 (Feb.)	–9 (Mar.)	–8 (Apr.)	–7 (May)	–6 (Jun.)	–5 (Jul.)	–4 (Aug.)	–3 (Sep.)	–2 (Oct.)	–1 (Nov.)
PCM	0.32[1)]	0.16	0.23[2)]	0.02	0.11	0.03	–0.17	–0.18	–0.01	–0.07	–0.08
SA1	0.14	0.03	0.01	–0.09	0.14	0.18	–0.09	–0.06	0.09	0.20	0.16
SA2	0.13	0.10	–0.07	–0.16	0.08	0.02	–0.07	–0.09	0.08	0.20	0.11
SB	0.23[2)]	–0.13	0.14	0.01	–0.05	–0.21	–0.23[2)]	–0.17	0.02	0.17	0.15
PN	0.20	–0.03	0.04	0.14	0.00	–0.12	–0.24[2)]	–0.25[2)]	–0.12	–0.02	0.12
SC	0.13	–0.02	0.14	–0.04	0.03	–0.09	–0.29[1)]	–0.27[1)]	–0.12	0.03	–0.01
SD	0.15	–0.10	0.21	0.18	0.13	–0.08	–0.33[1)]	–0.23[2)]	–0.04	0.14	0.17

Note: The negative signs in the column headings denote that the INT_g leads the winter EAMI, with the starting month given in brackets. [1)] correlations that exceed 95%; [2)] correlations that exceed 90%.

Table 3. Lag correlation coefficients of the INT_g with the winter EAMI

	0	+1 (Jan.)	+2 (Feb.)	+3 (Mar.)	+4 (Apr.)	+5 (May)	+6 (Jun.)	+7 (Jul.)	+8 (Aug.)	+9 (Sep.)	+10 (Oct.)
PCM	–0.05	0.22[2)]	0.14	–0.06	–0.32[1)]	0.03	–0.12	–0.23[2)]	–0.09	0.08	0.00
SA1	0.08	–0.12	0.09	–0.04	–0.18	–0.07	–0.05	–0.35[1)]	–0.10	–0.07	0.11
SA2	–0.14	–0.17	0.08	0.21	–0.02	0.03	0.07	–0.27[1)]	–0.14	–0.04	0.22[2)]
SB	0.05	–0.09	0.09	0.08	–0.07	–0.07	0.24[2)]	0.00	0.05	0.20	0.34[2)]
PN	0.02	0.05	0.04	–0.11	–0.20	–0.13	0.13	0.05	0.11	0.15	0.34[2)]
SC	0.04	0.12	0.32[1)]	0.04	–0.16	–0.22[2)]	0.01	–0.07	0.02	0.06	0.37[2)]
SD	0.04	0.10	0.26[1)]	0.10	–0.07	–0.10	0.12	–0.09	–0.11	0.00	0.38[2)]

Note: The positive signs in the column headings denote the INT_g lags the winter EAMI, with the starting month given in brackets. [1)] correlations that exceed 95%; [2)] correlations that exceed 90%.

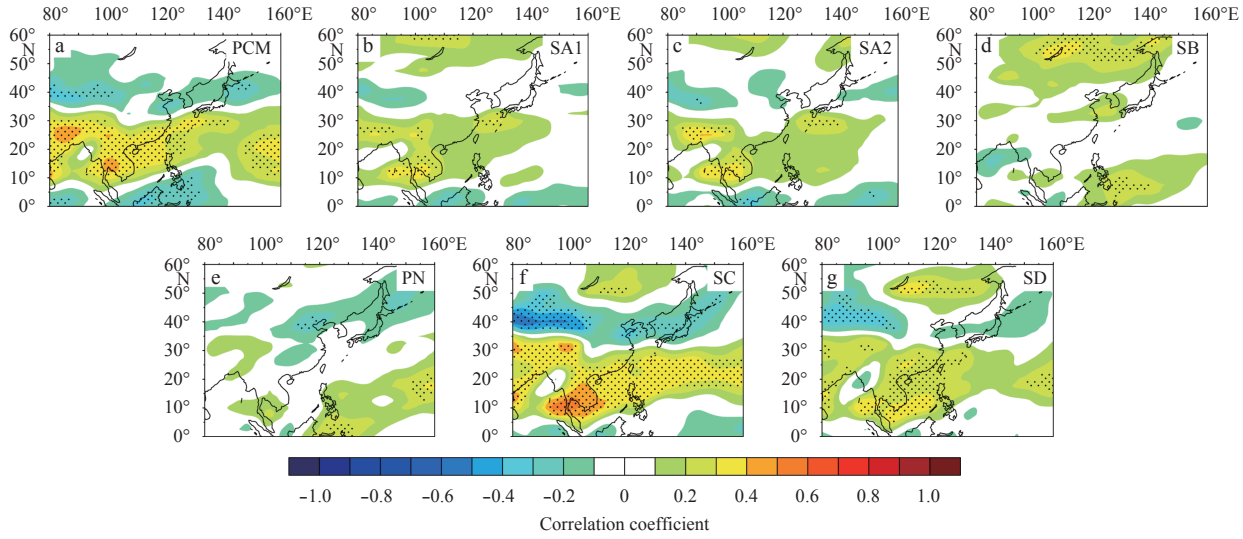

Fig. 3. Distribution of correlation coefficients between the winter southwest–northeast wind speed field and the 3-month average INT_g (February, March and April) at seven transects. The dot-shaded areas are significant at the 90% level.

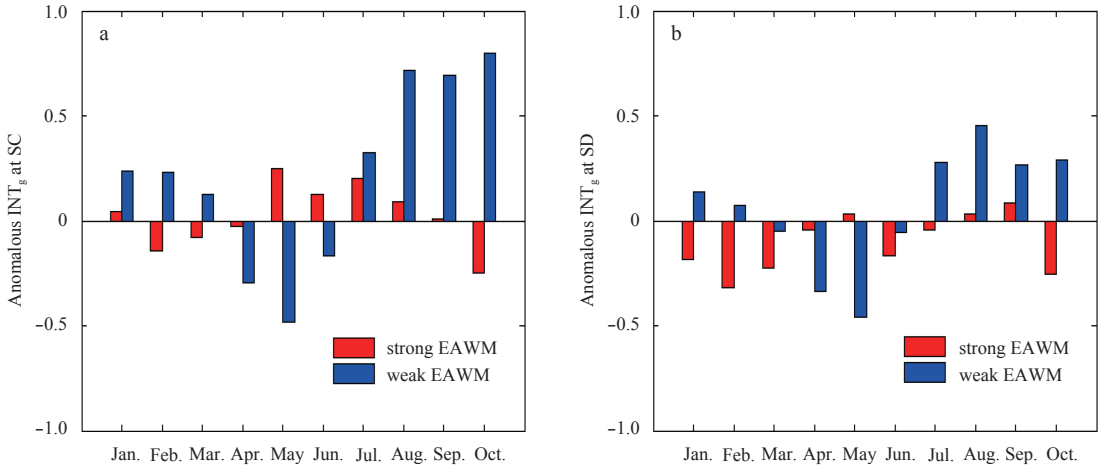

Fig. 4. Composites of the 3-month running mean INT_g anomaly (normalized) in the year following strong and weak EAWM conditions at Transects SC (a) and SD (b).

representative measure. Climatologically, the ΔT anomaly (SAT minus SST) over the Kuroshio is negative (Fig. 7a), with extremes centered in the downstream region. This distribution is reasonably similar to that of turbulent heat fluxes. When the winter monsoon is strong, the subsequent ΔT anomaly is negative (Fig. 7b), but the situation is reversed for weak cases (Fig. 7d). ΔT for strong cases is significantly smaller ($|\Delta T|$ is larger) than for weak cases, and the distribution also bears a resemblance to that in Fig. 5c, but with a reversed sign. On the other hand, the SST for strong conditions is not significantly lower than for weak conditions (figure omitted), nor is the distribution consistent with the first two elements (hear fluxes and ΔT). The dramatically cooled surface air in winter is thus seen to play the more important role in affecting turbulent fluxes. This finding implies that the primary factor in the EAWM is air–sea interaction along the Kuroshio in the ECS from February to April, generalized here as its thermal effect. A possible mechanism is as follows: higher wind speeds and $|\Delta T|$ during a strong winter monsoon increase turbulent heat fluxes vented by the ocean to the atmosphere. This corresponds to weak INT_g in the Kuroshio, especially downstream. On the contrary, wind speeds and $|\Delta T|$ are both weak during weak winter monsoons, and the resulting diminished heat fluxes are associated with a strong Kuroshio in the subsequent February–April period.

3.2.1.2 *Dynamic process*

To demonstrate further the influence of the winter monsoon on the Kuroshio, it is of interest to quantify whether the monsoon's dynamic effect is related to observed variations in the Kuroshio. Figure 8a shows the wind field climatology at 10 m and Sverdrup transport from February to April. This illustrates that, compared with the negative anomaly in adjacent areas, there is a positive band along the Kuroshio in the ECS, with extremes centered downstream. This means that the spatial distribution of wind-stress curl forces northward Sverdrup transport in the Kuroshio from February to April. The Sverdrup transport is calculated using the following formula:

$$M_y = \frac{1}{\beta}\mathrm{curl}\tau,$$

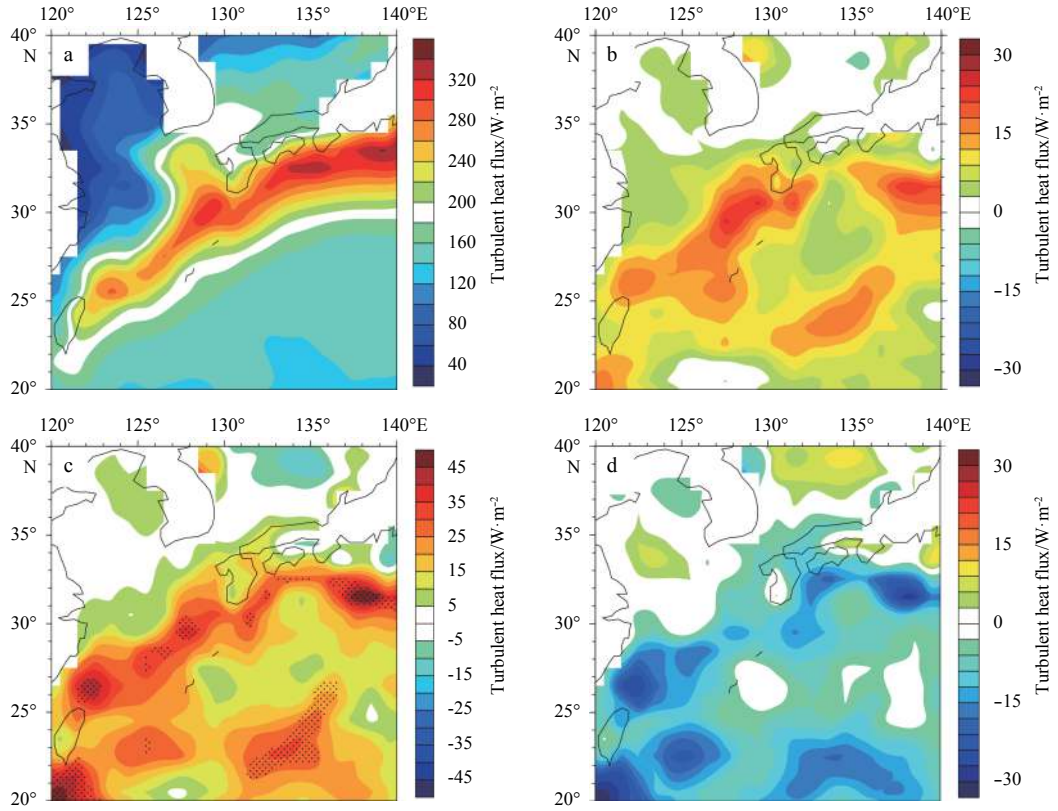

Fig. 5. Composites of turbulent heat fluxes for different winter monsoon conditions. a. Average turbulent heat fluxes (upward positive) in the Kuroshio and adjacent waters from February to April; b. composite of turbulent heat flux anomalies for strong winter monsoons; c. composite difference of turbulent heat fluxes between strong and weak winter monsoons; dotted areas are significant at 90%; and d. same as Fig. 5b, but for weak winter monsoons.

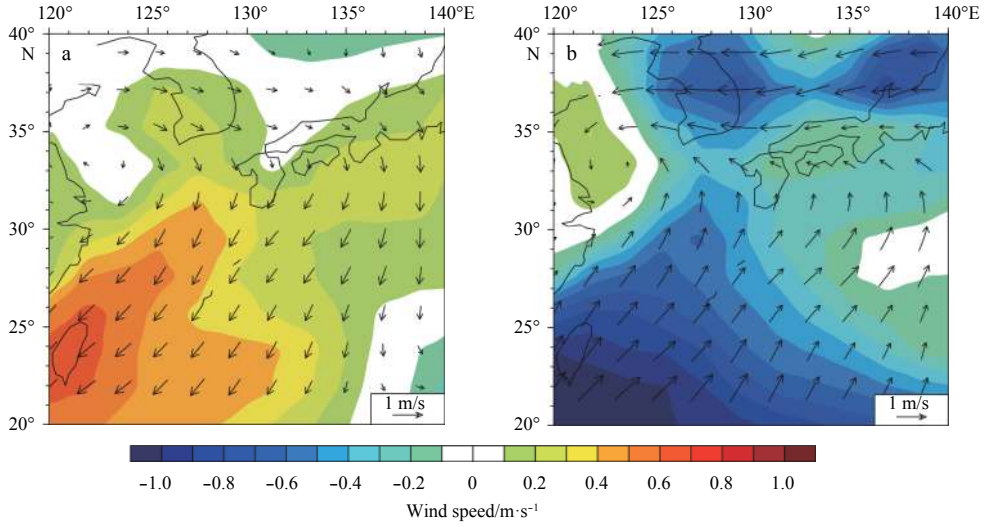

Fig. 6. Composite of wind speed (color tones) and wind field (vectors) anomalies from February to April following strong winter monsoons (a), and same as a but for weak winter monsoons (b).

where $\beta \equiv (\mathrm{d}f/\mathrm{d}y)_{\Phi_0} = 2\Omega\cos\Phi_0/a$. As generally understood, because of the friction force in western boundary currents, the Sverdrup model is not technically applicable. However, the distribution of Sverdrup transport driven by the wind field can still be used as a sketch map, to observe change in the Kuroshio.

Figure 8b presents the composite difference between strong and weak winter monsoon conditions of Sverdrup transport in the following early spring. When the winter monsoon is anomalously strong (weak), the subsequent transport is larger (smaller). This means that with respect to weak cases, the strong monsoon intensifies northward Sverdrup transport, and the Kuroshio is enhanced accordingly. Although this result fails to agree with the earlier correlation analysis, the disagreement can be understood by considering that the INT_g is derived from sea-surface data,

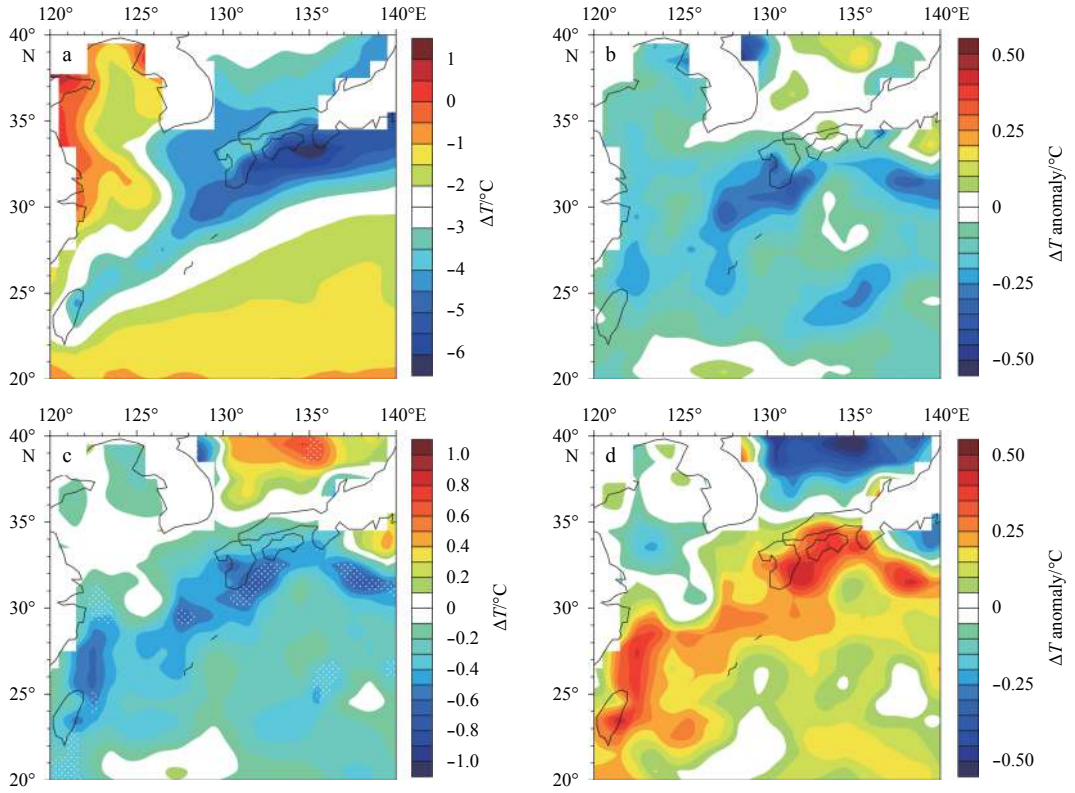

Fig. 7. Composites of ΔT for different winter monsoon conditions. a. Average ΔT over the Kuroshio and adjacent waters from February to April; b. composite of the ΔT anomaly from February to April following strong winter monsoons; c. composite difference of ΔT between strong and weak winter monsoons; dotted areas are significant at 90%; and d. same as Fig. 7b, but for weak winter monsoons.

while Sverdrup transport reflects the overall transport volume in the layer of wind-driven ocean circulation.

Now the process that weakens the surface Kuroshio INT_g downstream will be explored. If it is not the wind stress curl that reflects non-local influences, can it be the local wind field instead? To address these questions, Ekman transport along the Kuroshio was calculated, because it is dependent on the local wind field. In the Northern Hemisphere, the direction of Ekman transport is perpendicular and to the right of the wind stress. Figure 8c presents the climatological distribution. There is northwesterly wind in the downstream region (vectors in Fig. 8a), where southwestward-forced Ekman transport opposes the Kuroshio current direction. In the upstream region, however, the wind direction changes to the northeast and the Ekman transport becomes northwestward. The composite difference between strong and weak winter monsoons of Ekman transport from February to April is given in Fig. 8d. When the winter monsoon strengthens (weakens), there is strong (weak) southwest Ekman transport downstream, which weakens the INT_g at transects SC and SD. The result is coincident with that in Fig. 3, and explains why the INT_g at downstream transects is more notably weakened by the wind field. Thus, the dynamic effect of the winter monsoon is another of the factors that affect the Kuroshio INT_g in the ECS in the early spring, brought about by altering the local Ekman transport.

In summary, the winter monsoon subsequently affects the Kuroshio through both thermal and dynamic processes. Through midlatitude tropical interaction, the winter monsoon spreads its influence to the global scale (Chen et al., 2000). Compared with the monsoon, the Kuroshio is small in spatial scale. The differences in scale mean that the interactions between the winter monsoon and the Kuroshio INT_g are aided by processes with a smaller spatial scale–local wind stress and heating at the sea surface.

3.2.2 *Impacts of the EAWM on the Kuroshio intensity in the ECS in the following early winter*

The winter EAMI is significantly correlated with the 10-month-lag INT_g at all observation transects except PCM and SA1. The spatial distribution of correlation coefficients between the winter wind-speed field and the INT_g from October to December in the following year at the seven transects is mapped in Fig. 9. It shows that all transects other than PCM have high positive correlations in the monsoon region. This means that when the anomalous southwesterly winds intensify (winter monsoon weakens), the INT_g in the midstream and downstream Kuroshio is strong, and vice versa. The October–December INT_g composites for strong and weak winter monsoons (SC and SD are shown in Fig. 3; other figures omitted) reveal that the INT_g is weaker in strong winter monsoons than in weak monsoons. How then does the winter monsoon influence the Kuroshio in the subsequent early winter? Is there any difference from the mechanisms during the February–April period discussed above? This will be explored in the following section.

3.2.2.1 *Thermal process*

First, the thermal process will be discussed. Composites of turbulent heat fluxes for different winter monsoon conditions are

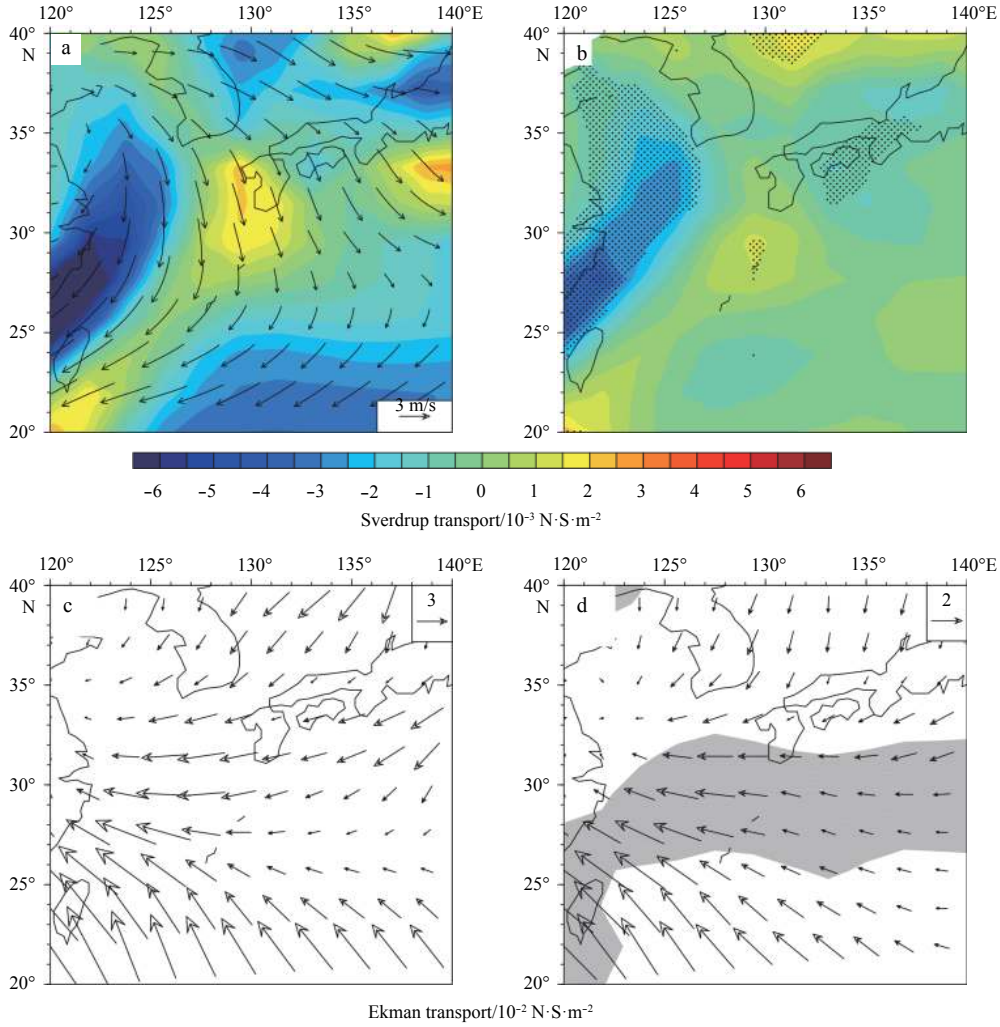

Fig. 8. Composites of Sverdrup transport for different winter monsoon conditions. a. Average Sverdrup transport (color tones) and wind field (vectors) across the Kuroshio and adjacent waters from February to April; b. composite difference between strong and weak winter monsoons of Sverdrup transport in the following February–April period; dot-shaded areas are significant at 90%; c. same as a but for Ekman transport; and d. same as Fig. 8b, but for Ekman transport; shaded areas are significant at 90%.

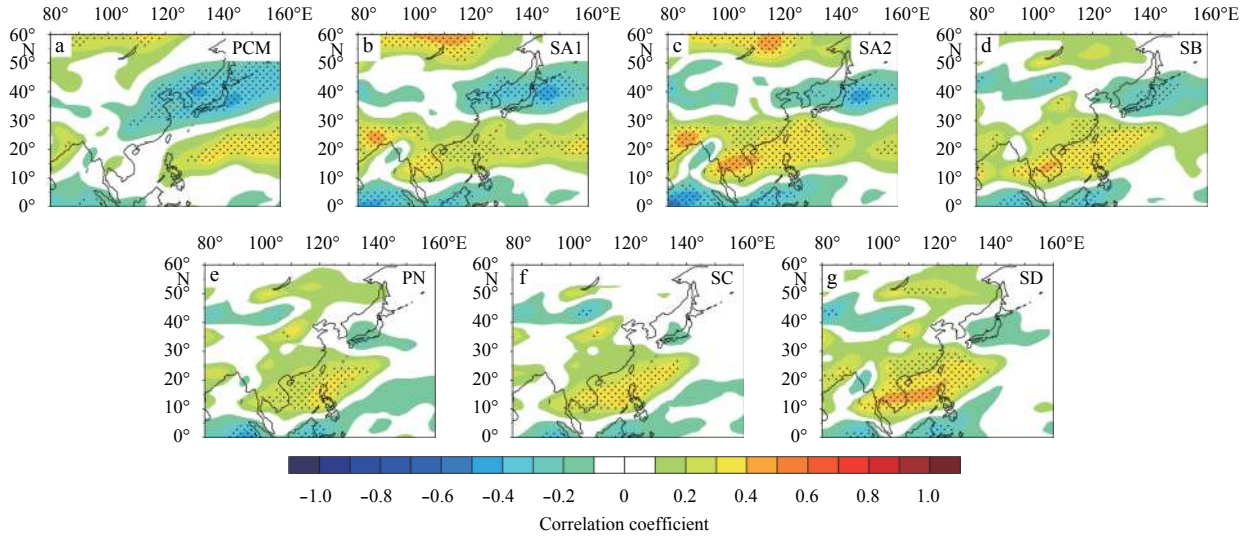

Fig. 9. Distribution of correlation coefficients between the winter southwest–northeast wind speed field and the 3-month average INT_g (October, November and December) in the following year at seven transects. The dot-shaded areas are significant at 90%.

plotted in Fig. 10. The high-value belt where the Kuroshio releases much more heat to the atmosphere still exists (Fig. 10a). Under strong winter monsoon conditions, a negative anomaly covers the Kuroshio in the ECS, and thus the Kuroshio releases less turbulent heat flux to the atmosphere in the following October–December period (Fig. 10b). In addition, the extremes centered in the southeast downstream region deviate from the Kuroshio main axis. For weak monsoons, the anomaly is positive and the Kuroshio in the ECS releases more heat to the atmosphere (Fig. 10d). The extremes are also centered downstream. However, the result is opposite to the distribution from February to April (Figs 5b to d).

During the two periods examined, there are similar positive correlations with the winter EAMI. However, the composite results are opposite. Is atmospheric forcing still dominant from October to December, similar to the February–April situation? To figure out this question, composite analyses for variables concerned were performed.

Composite analysis shows that under strong winter monsoon conditions, there is a slight easterly anomaly over the Kuroshio. Under weak winter monsoon conditions, there is an anomalous northwesterly. The wind speeds are both positive anomalies with no significant difference (figure omitted). As seen from the composites of the ΔT over the Kuroshio, there is a positive anomaly under strong winter monsoons (Fig. 11b), and a negative anomaly under weak monsoons (Fig. 11d). The difference is not significant, but their distributions are similar to those of turbulent heat fluxes. Composites of SST along the Kuroshio illustrate that SST from October to December after a strong winter monsoon are lower than after a weak monsoon (Fig. 12c), and that the distribution is analogous to both ΔT and turbulent heat fluxes.

These composite results suggest a possible mechanism: from October to December in the year following the winter monsoon, oceanic forcing dominates the local air–sea interaction processes over the Kuroshio in the ECS. This means that after a strong winter monsoon, the weakened Kuroshio (corresponding to lower SST) releases less heat to the atmosphere from October to December. The decreased heating reduces the land–sea thermal contrast, which in turn weakens the subsequent winter monsoon. In contrast, after a weak winter monsoon, the strengthened Kuroshio (corresponding to higher SST) releases more heat to the atmosphere from October to December. This enhances the land–sea thermal contrast, which in turn strengthens the subsequent winter monsoon.

At present, there are two problems with the mechanism. One is how the winter monsoon affects the 10-month-lag INT_g; the other is why the primary factor influencing the air–sea interaction changes. Li et al. (2010) proposed that the East Asian monsoon has a tropospheric biennial oscillation (TBO), such that a strong winter monsoon precedes a weak winter monsoon. Here, through the oscillation, a strong winter monsoon may induce a weak INT_g in the midstream and downstream Kuroshio over the following October–December for a 2 a period. Due to the subsequent weakening of the winter monsoon, atmospheric forcing loses its dominance in the air–sea interaction, being replaced by oceanic forcing instead. Thus, the INT_g has an impact on the strength of the winter monsoon (as previously described), which completes a positive feedback mechanism. One point should be

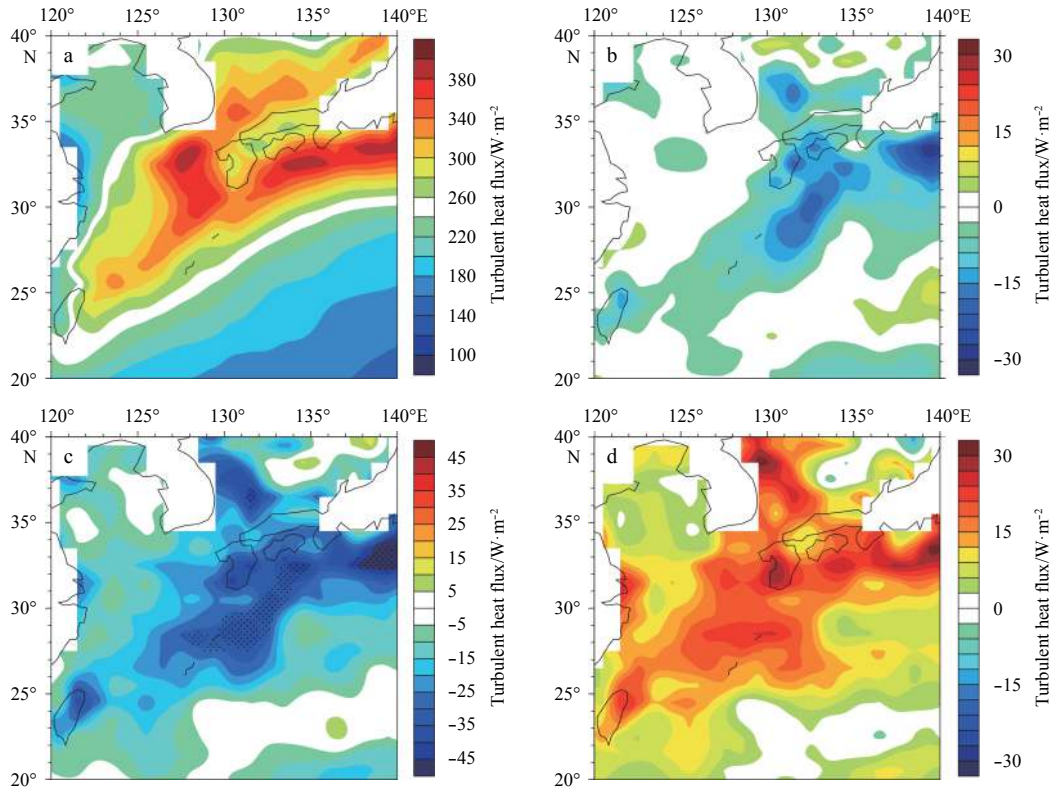

Fig. 10. Composites of turbulent heat fluxes for different winter monsoon conditions. a. Average turbulent heat fluxes (upward positive) across the Kuroshio and adjacent waters from October to December; b. composite turbulent heat flux anomalies from October to December in the year following strong winter monsoons; c. composite difference of turbulent heat fluxes between strong and weak winter monsoons; dotted areas are significant at 90%; and d. same as Fig. 10b, but for weak winter monsoons.

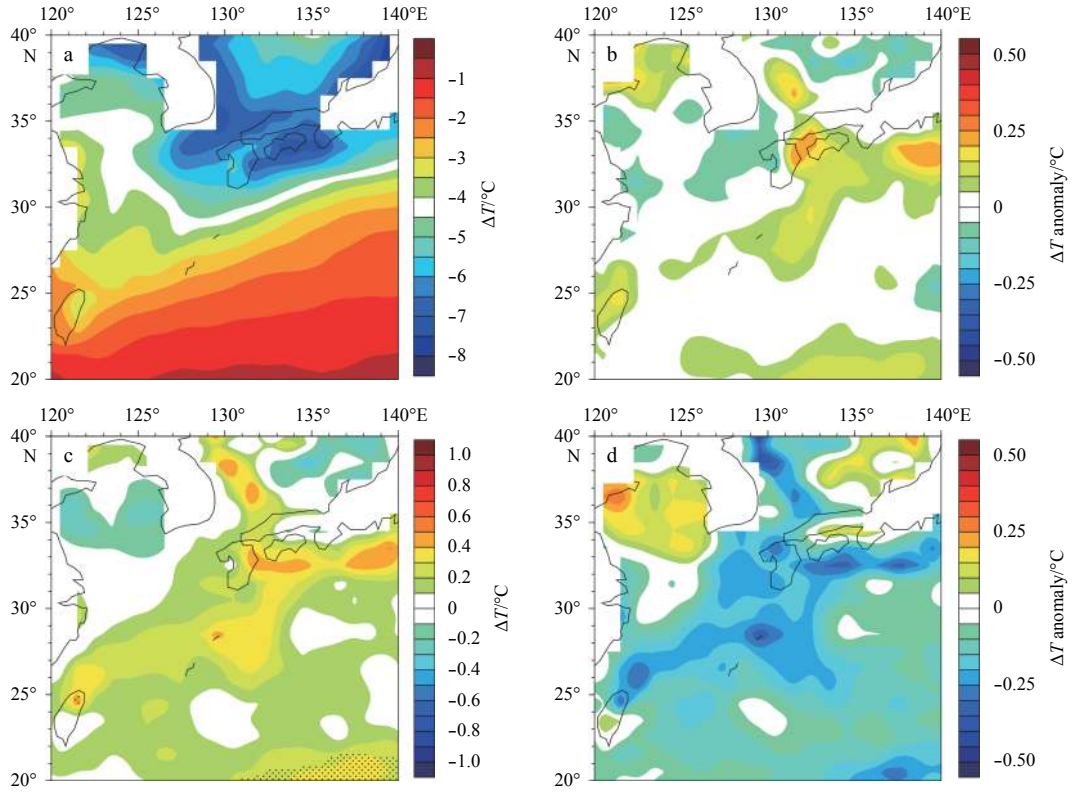

Fig. 11. Composites of ΔT for different winter monsoon conditions. a. Average ΔT over the Kuroshio and adjacent waters from October to December; b. composite of the ΔT anomaly from October to December in the year following strong winter monsoons; c. composite difference of ΔT between strong and weak winter monsoons; dotted areas are significant at 90%; and d. same as Fig. 11b, but for weak winter monsoons.

noted regarding this mechanism: whether atmospheric or oceanic forcing is the dominant process in the air–sea interaction of the Kuroshio in the ECS is determined by the relative strength of the EAWM and the INT_g. The INT_g in the early winter after a strong winter monsoon is weak, with its subsequent winter monsoon weaker. Under weak winter monsoon conditions, the following winter monsoon is strong, but the INT_g over the next October–December is stronger. Oceanic forcing is therefore dominant in both cases. To summarize, there may be a "critical value" in the relative strength of the EAWM and the INT_g that determines the conversion between atmospheric and oceanic forcings.

3.2.2.2 *Dynamic process*

Composite differences of both Sverdrup transport and Ekman transport along the Kuroshio in the ECS from October to December after strong and weak winter monsoons fail to pass the significance test (figure omitted). Results indicate that the dynamic process of the EAWM cannot be directly responsible for the interannual change in the Kuroshio in the ECS for the October–December period. This is because the influence of local and non-local wind stresses on the Kuroshio in the ECS is not as great on the interannual timescale as on the seasonal timescale (Yu et al., 2008). To conclude, the dynamic effect of the winter monsoon is not a dominant process. This result echoes the finding of the previous section that, from October to December, oceanic forcing is the main process in the Kuroshio in the ECS.

4 Discussion and conclusions

Based on satellite altimeter data and reanalysis data, the relationships between the Kuroshio intensity in the ECS and the East Asian winter monsoon are examined. Their possible interaction mechanisms are also discussed.

Variability in the Kuroshio in the ECS ranges over periods of days to years. Transects in close proximity vary in a similar way, while great differences exist between upstream, midstream and downstream regions of the Kuroshio. Correlation between midstream and upstream locations is not as significant as that between midstream and downstream locations.

On the interannual timescale, there is an interaction between the Kuroshio in the ECS and the winter monsoon. When the winter monsoon strengthens, the INT_g weakens at transects SC and SD over the following February–April period. The situation is reversed for weak monsoons. The phenomenon is caused by both dynamic and thermal effects of the winter monsoon. The monsoon produces its dynamic effect by influencing Ekman transport. The thermal effect following a strong winter monsoon is that greater wind speed and $|\Delta T|$ cause the ocean to release more heat to the atmosphere, which weakens the Kuroshio INT_g, especially downstream. Under weak monsoons with lower wind speed and $|\Delta T|$, the ocean vents less heat to the atmosphere, coinciding with enhanced INT_g. During the February–April period, atmospheric forcing is therefore dominant.

When the winter monsoon strengthens (weakens), the midstream and downstream Kuroshio INT_g is also suppressed (enhanced) in the following October–December period. This process differs from that in early spring. Because of the TBO, a strong winter monsoon usually precedes a weak monsoon, and reduces the INT_g during the following October–December. Oceanic for-

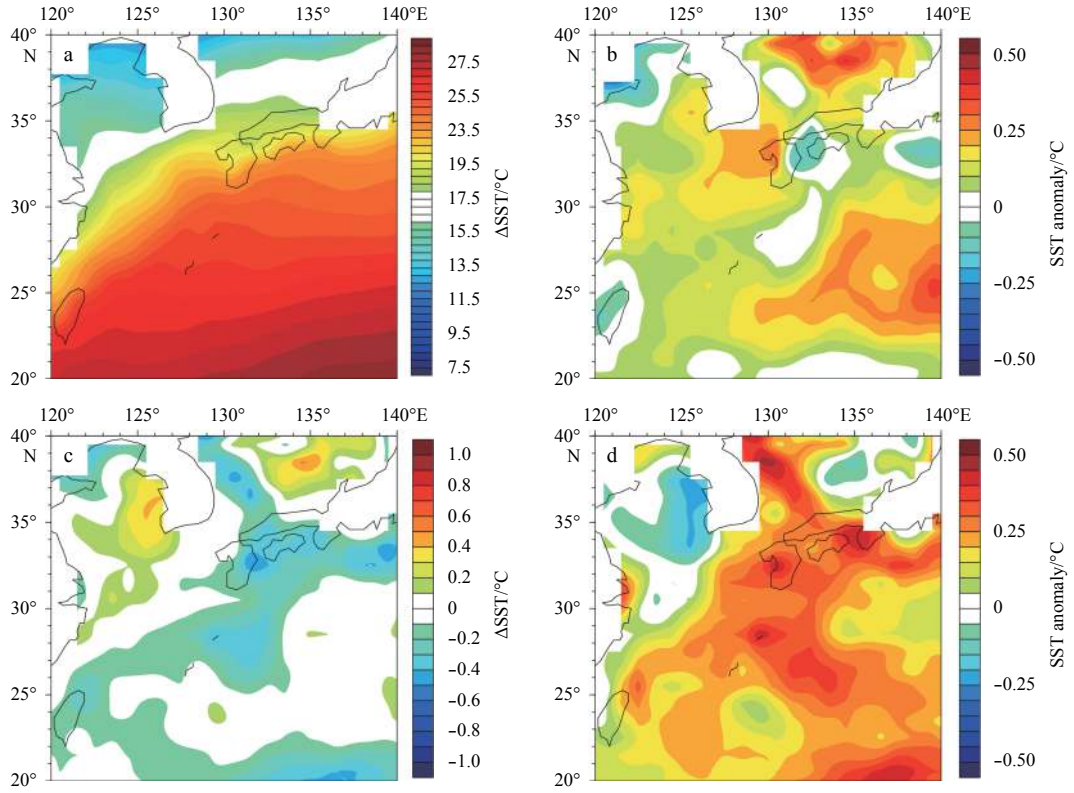

Fig. 12. Composites of SST for different winter monsoon winter conditions. a. Average SST across the Kuroshio and adjacent waters from October to December; b. composite of the SST anomaly from October to December in the year following strong winter monsoons; c. composite difference of SST (ΔSST) between strong and weak winter monsoons; and d. same as Fig. 12b, but for weak winter monsoons.

cing takes on the leading role during this period. Consequently, a weak Kuroshio (corresponding to a lower SST) releases less heat into the atmosphere from October to December after a strong winter monsoon, and in turn reduces the land–sea thermal contrast and weakens the subsequent winter monsoon. In contrast, after a weak winter monsoon, the INT_g in the following October–December is anomalously strong (corresponding to higher SST), increasing heat transfer to the atmosphere. This enhances the land–sea thermal contrast, which in turn strengthens the subsequent winter monsoon.

Together these analyses present a complete positive feedback system, including both atmospheric and oceanic coupling processes. The schematic diagram in Fig. 13 illustrates the cycle, and describes the basic characteristics of the interaction between the EAWM and intensity of the Kuroshio in the ECS. During early winter, as determined by the relative strengths of the winter monsoon and the Kuroshio in the ECS, the dominant process over the Kuroshio is oceanic forcing, different from conditions typical in early spring when atmospheric forcing dominates. A "critical value" may determine the conversion from atmospheric to oceanic forcing processes.

The non-equivalence in spatial scales between the EAWM and the Kuroshio means that processes with a small spatial scale (i.e., local wind stress and heating at the sea surface) must contribute to their interactions. Finally, air–sea interaction along the Kuroshio is complex and the physical mechanism of the TBO that influences the INT_g has not been well described. Numerical tests will be necessary to corroborate the results of observational analysis presented here.

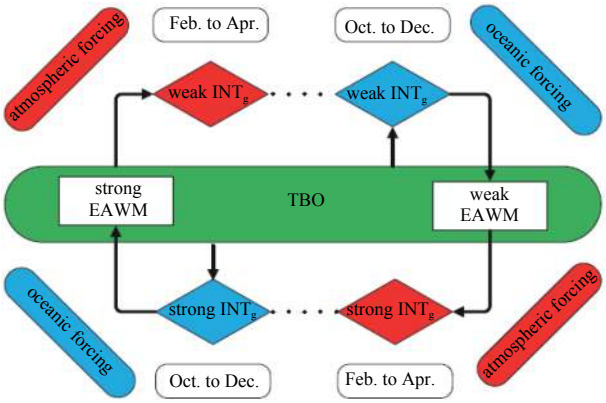

Fig. 13. A schematic diagram of the interaction between the EAWM and the Kuroshio INT_g in the ECS. The red color indicates where atmospheric forcing is dominant, blue represents oceanic forcing, and green denotes the role of TBO.

References

Cayan D R. 1992. Latent and sensible heat flux anomalies over the northern oceans: driving the sea surface temperature. J Phys Oceanogr, 22(8): 859–881

Chang Y L, Oey L Y. 2011. Interannual and seasonal variations of Kuroshio transport east of Taiwan inferred from 29 years of tide-gauge data. Geophys Res Lett, 38(8): L08603

Chang Y L, Oey L Y. 2012. The Philippines-Taiwan oscillation: monsoonlike interannual oscillation of the subtropical-tropical western north Pacific wind system and its impact on the ocean.

J Climate, 25(5): 1597–1618
Chao S Y. 1990. Circulation of the East China Sea, a numerical study. J Oceanogr, 46(6): 273–295
Chen Wen, Graf H F, Huang Ronghui. 2000. The interannual variability of East Asian Winter Monsoon and its relation to the summer monsoon. Adv Atmos Sci, 17(1): 48–60
Chen Longxun, Zhang Bo, Zhang Ying. 2006. Progress in research on the East Asian monsoon. J Appl Meteor Sci (in Chinese), 17(6): 711–724
Chuang W S, Liang W D. 1994. Seasonal variability of intrusion of the Kuroshio water across the continental shelf northeast of Taiwan. J Oceanogr, 50(5): 531–542
Hsin Y C, Qiu Bo, Chiang T L, et al. 2013. Seasonal to interannual variations in the intensity and central position of the surface Kuroshio east of Taiwan. J Geophys Res: Oceans, 118(9): 4305–4316
Hu Dunxin, Wu Lixin, Cai Wenju, et al. 2015. Pacific western boundary currents and their roles in climate. Nature, 522(7556): 299–308
Huang Ruixin. 2012. Ocean Circulation: Wind-Driven and Thermohaline Processes (in Chinese). Le Kentang, Shi Jiuxin, trans. Beijing: Higher Education Press, 731
Johns W E, Lee T N, Zhang Dongxiao, et al. 2001. The Kuroshio east of Taiwan: Moored transport observations from the WOCE PCM-1 array. J Phys Oceanogr, 31(4): 1031–1053
Li Yuefeng, Ding Yihui. 2002. Sea surface temperature, land surface temperature and the summer rainfall anomalies over Eastern China. Climatic Environ Res (in Chinese), 7(1): 87–101
Li Chongyin, Pan Jing, Que Zhiping. 2011a. Variation of the East Asian Monsoon and the tropospheric biennial oscillation. Chin Sci Bull, 56(1): 70–75
Li Bo, Zhou Tianjun, Lin Pengfei, et al. 2011b. The wintertime North Pacific surface heat flux anomaly and air-sea interaction as simulated by the LASG/IAP ocean-atmosphere coupled model FGOAL_s1.0. Acta Meteor Sin (in Chinese), 69(1): 52–63
Liang Qiaoqian, Jian Maoqiu, Peng Zhigang, et al. 2006. Impacts of East Asian winter monsoon on sea surface temperature in northwestern Pacific. Journal of Tropical Oceanography (in Chinese), 25(6): 1-7
Oey L Y, Hsin Y C, Wu C R. 2010. Why does the Kuroshio northeast of Taiwan shift shelfward in winter? Ocean Dyn, 60(2): 413–426
Qin Zhengkun, Sun Zhaobo. 2006. Influence of abnormal East Asian winter monsoon on the northwestern Pacific sea temperature. Chin J Atmos Sci (in Chinese), 30(2): 257–267
Qiu Bo. 1999. Seasonal eddy field modulation of the north Pacific Subtropical Countercurrent: TOPEX/Poseidon observations and theory. J Phys Oceanogr, 29(10): 2471–2486
Qiu Bo, Chen Shuiming. 2010. Interannual variability of the North Pacific subtropical countercurrent and its associated mesoscale eddy field. J Phys Oceanogr, 40(1): 213–225
Qiu Bo, Chen Shuiming. 2013. Concurrent decadal mesoscale eddy modulations in the western North Pacific subtropical gyre. J Phys Oceanogr, 43(2): 344–358
Soeyanto E, Guo Xinyu, Jun O, et al. 2014. Interannual variations of Kuroshio transport in the East China Sea and its relation to the Pacific Decadal Oscillation and mesoscale eddies. J Geophys Res: Oceans, 119(6): 3595–3616
Wallace J M, Jiang Q. 1987. On the observed structure of the interannual variability of the atmosphere-ocean climate system. In: Cattle H, ed. Atmospheric and Oceanic Variability. Bracknell: Royal Meteorological Society, 17–43
Wang Zheng, Yuan Dongliang, Hou Yijun. 2010. Effect of meridional wind on gap-leaping western boundary current. Chin J Oceanol Limnol, 28(2): 354–358
Wijffels S, Firing E, Toole J. 1995. The mean structure and variability of the Mindanao Current at 8°N. J Geophys Res, 100(C9): 18421–18435
Xu Haiming, Wang Linwei, He Jinhai. 2008. Observed oceanic feedback to the atmosphere over the Kuroshio Extension during spring time and its possible mechanism. Chin Sci Bull, 53(12): 1905–1912
Xu Haiming, Xu Mimi, Xie Shangping, et al. 2011. Deep atmospheric response to the spring Kuroshio over the East China Sea. J Climate, 24(18): 4959–4972
Yang Y, Liu C T, Hu J H, et al. 1999. Taiwan current (Kuroshio) and impinging eddies. J Oceanogr, 55(5): 609–617
Sasaki Y N, Minobe S, Asai T, et al. 2012. Influence of the Kuroshio in the East China Sea on the early summer (Baiu) rain. J Climate, 25(19): 6627–6645
Yu Lisan, Weller R A. 2007. Objectively analyzed air-sea heat Fluxes for the global ice-free oceans (1981-2005). Bull Am Meteor Soc, 88(4): 527–539
Yu Fan, Wang Qi, Liu Yulong. 2008. The seasonal and interannual variations of the upper Kuroshio circulation in the East China Sea and their relationship with local wind stress. Periodical of Ocean University of China (in Chinese), 38(4): 533–538
Zhang Qilong, Hou Yijun, Qi Qinghua. 2008. Variations in the Kuroshio heat transport in the East China Sea and meridional wind anomaly. Adv Marine Sci (in Chinese), 26(2): 126–134